Nano Research 2018, 11(10): 5499–5518
https://doi.org/10.1007/s12274-018-2073-1
Review Article
ISSN 1998-0124
CN 11-5974/O4

Recent progress in background-free latent fingerprint imaging

Yingqian Wang, Jie Wang, Qinqin Ma, Zhihao Li, and Quan Yuan (✉)

Key Laboratory of Analytical Chemistry for Biology and Medicine (Ministry of Education), College of Chemistry and Molecular Sciences, Wuhan University, Wuhan 430072, China

Received: 10 March 2018
Revised: 10 April 2018
Accepted: 13 April 2018

KEYWORDS
latent fingerprints, background interference, upconversion, persistent luminescence, nanoparticles

ABSTRACT

Owing to their unique pattern and abundant chemical composition, latent fingerprints (LFPs) can serve as "ID cards" and "information banks" of donors and therefore are valuable for forensic investigation, access control, and even medical diagnosis. LFP imaging has attracted considerable attention, and a great variety of contrast agents has been developed. In LFP imaging, background signals such as background fluorescence from the underlying surface can seriously blur the LFP images and decrease imaging sensitivity; thus, great efforts have been made to eliminate background interference. Here, we stratify the recent progress in background-free LFP imaging by making use of the difference in properties between contrast agents and background compounds. For example, near-infrared (NIR) light-activatable contrast agents can efficiently remove background signals in LFP imaging because the background compounds cannot be excited by NIR light, showing that the difference in excitation properties between contrast agents and background compounds can be employed to eliminate background interference. This review is organized around background-free LFP imaging based on the difference in optical properties between contrast agents and background compounds: (i) different excitation wavelengths, (ii) different emission wavelengths, (iii) different luminescence lifetime values, (iv) different plasmonic properties, (v) different photothermal properties, and (vi) different electrochemiluminescence properties.

1 Introduction

The patterns of friction ridge skin are formed by certain raised portions of the epidermis on the fingertips, palms, and soles of an individual [1, 2]. They are genotypically determined, unique, and persistent [1, 3], which enable them to serve for individual identification in various practical applications, such as criminal investigation, authority control, and information encryption [4]. Generally speaking, when a finger touches a surface, the secretions present on the surface of the skin are transferred onto the substrate, resulting

Address correspondence to yuanquan@whu.edu.cn

in an impression of the friction ridge pattern [1, 5]. Most of the impressions are invisible to the naked eye and are called latent fingerprints (LFPs). LFPs not only reproduce the physical characteristics of an individual's ridge patterns but also contain heterogeneous chemical components [6, 7]. Generally, LFPs contain a mixture of intrinsic and extrinsic constituents. The intrinsic components of a fingerprint are mainly secreted by the natural secretion glands, such as exocrine sweat glands and sebaceous glands. Extrinsic constituents mainly originate from the various available contaminants, such as make-up, food contaminants, blood, dirt, and grease. The differences among donors, such as gender, age, medication use, metabolism, diet, and surroundings, can result in the variations of fingerprint composition [6]. Analysis of these fingerprint compositions can offer enormous information about the donor. As a result, LFPs can serve as an information storage platform for individuals and play an important role in forensic investigation, medical diagnostics, and health assessment.

LFP imaging has attracted considerable attention. The basic principle of LFP imaging is to establish a contrast between the secretion residues and the substrates bearing them [5]. LFP imaging enables direct visualization of an LFP pattern and the detailed features for individual identification, which is important in crime scene and forensic applications. More importantly, the imaging of compounds of interest in LFPs, such as metabolites or contaminants, provides the opportunity to obtain valuable information for the applications including metabolism analysis and safety inspection. In the past decades, dozens of contrast agents and imaging techniques have been developed for LFP imaging [4, 7–12]. Regardless of the contrast agents or imaging techniques used, there are some problems that seriously affect the sensitivity and resolution of LFP imaging (and need to be considered): mostly the interference caused by background signals [12]. The substrates bearing LFPs usually contain background compounds that possess properties similar to those of the contrast agents. As a result, these compounds can produce strong background signals in LFP imaging and thereby severely decrease imaging sensitivity and resolution. Consequently, how to avoid background interference has aroused broad interest.

Up to now, a number of reviews emphasizing LFP imaging have been published. For example, Russell et al. [1] have highlighted the advances in fingerprinting technology that can simultaneously provide chemical information and individual identification. Zhang et al. [3] have summarized the chemical methods that can provide chemical information on LFPs. Bécue et al. [5] have introduced the methods for LFP detection from the forensic perspective and biological/chemical considerations. These reviews mainly focus on the information extraction and analysis of LFPs. The LFP imaging methods that can eliminate the background interference are seldom discussed. In this review, we summarize the recent progress in background-free LFP imaging over the past few years. We stratify the methods for eliminating background signals with respect to the difference in properties between the contrast agents and background compounds. Specifically, the review is divided into six sections around background-free LFP imaging according to the difference in properties between the contrast agents and background compounds: (i) different excitation wavelengths, (ii) different emission wavelengths, (iii) different luminescence lifetime values, (iv) different plasmonic properties, (v) different photothermal properties, and (vi) different electrochemiluminescent properties.

2 LFP imaging based on different excitation wavelengths

Background fluorescence is one of the most frequently encountered types of background interference in LFP imaging. Background fluorescence originates from coexcitation of the contrast agents attached to LFPs and the background chromophores in the underlying substrates [13], suggesting that the extent of background fluorescence interference is associated with the excitation wavelength. Contrast agents that can be excited at a wavelength significantly different from that of background chromophores are ideal candidates to reduce the background fluorescence interference. With excitation red-shifted, background fluorescence interference gradually decreases [14]. Near-infrared (NIR) light might represent an ideal light source to eliminate background fluorescence because the

vast majority of background chromophores cannot be excited by NIR light [15, 16]. Thus, contrast agents excited in the NIR region are ideal for background-free LFP imaging.

Upconversion nanoparticles (UCNPs) are some of the representative NIR-excited phosphors [17–21]. Upconversion is a definite anti-Stokes process in which two or more low-energy continuous-wave NIR photons are converted into a higher energy output photon [22]. The LFP imaging enhanced with UCNPs suffers little from background fluorescence interference under NIR excitation, thus providing high contrast and improving detection sensitivity [23–31]. What is more, the luminescent color of UCNPs can be fine-tuned by changing the type and concentration of the ions used for doping, thus allowing for multicolor imaging [25]. Additionally, UCNPs offer benefits of remarkable physicochemical stability and superior photostability without on-off blinking [22]. Above all, UCNPs are ideal candidates for background-free LFP imaging.

2.1 UCNP colloid dispersion for LFP imaging

In 2014, our group demonstrated the potent ability of UCNPs to eliminate background fluorescence interference for LFP imaging [24]. In that study, we developed a general and easy-to-use method for background-free LFP imaging based on lysozyme-binding aptamer (LBA)-modified UCNPs (UCNPs-LBA). Lysozyme is an important polypeptide component of human sweat, playing a pivotal part in protection of the skin. The strategy for LFP imaging with UCNPs-LBA is illustrated in Fig. 1(a). The UCNPs-LBA imaging probe can bind to fingerprint ridges through the specific recognition of lysozyme by the aptamer. A clear-cut green LFP image could be obtained under the excitation by a portable NIR laser with emission at 980 nm. As shown in Figs. 1(b) and 1(c), obvious background fluorescence interference could be observed when the LFPs were treated with imaging probes based on organic dyes and quantum dots (QDs) because of coexcitation of the two contrast agents and the background chromophores in substrates. In contrast, as presented in Fig. 1(d), the LFPs treated with UCNPs suffer little from the background fluorescence interference because the background chromophores cannot be excited by NIR light. Thus, a sharp LFP image with high resolution and high contrast was observed.

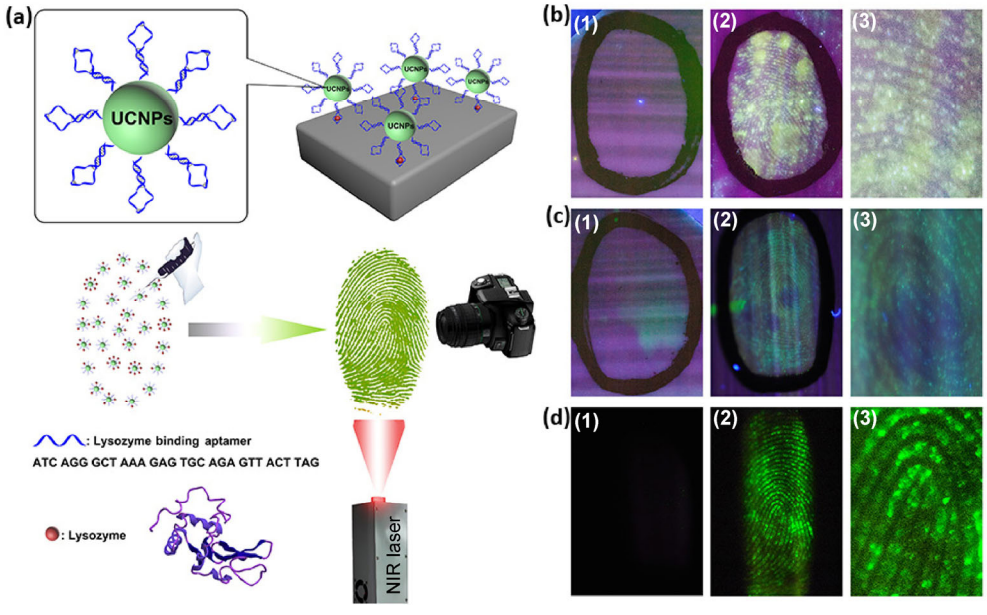

Figure 1 (a) Schematic illustration of simultaneous LFP imaging and lysozyme detection using UCNPs functionalized with a lysozyme-binding aptamer nanoconjugate. (b) A luminescence image of fingerprints treated with a FAM solution (1), FAM-LBA (2), and the corresponding magnified image (3). (c) A luminescence image of fingerprints treated with a QD solution (1), QDs-LBA (2), and the corresponding magnified image (3). (d) A luminescence image of fingerprints treated with a PAA-UCNP solution (1), UCNPs-LBA (2), and the corresponding magnified image (3). Reproduced with permission from Ref. [24], © John Wiley & Sons 2014.

More importantly, we next expanded this strategy for cocaine detection in LFPs by replacing LBA with a cocaine-binding aptamer. Similarly, the strategy can be applied to the detection of various kinds of chemicals in LFPs by simply altering the type of the aptamer. Moreover, the design gives tremendous opportunities both for LFP imaging and practical applications.

Later, Wang et al. [25] developed a surfactant-assisted method for LFP imaging with a UCNP colloid dispersion. The LFPs were immersed into a suspension containing UCNPs and the surfactant sodium dodecyl sulfate (SDS). The amphiphilic SDS could link hydrophilic UCNPs to hydrophobic grease in LFP residues. After illumination with 980 nm NIR light, the LFPs could be visualized without the interference of background fluorescence. LFP imaging was realized on various substrates. Additionally, multicolored LFP luminescence images were also obtained by changing the type and concentration of rare earth ions employed for doping.

2.2 UCNP powder for LFP imaging

The above-mentioned LFP imaging is conducted by solution-based imaging methods. The following studies are about background-free LFP imaging with the powder dusting technique. Mao et al. [27] have used $NaYF_4$:Yb,Er UCNP powders as a luminescent label for LFP imaging with low background interference, high contrast, and improved sensitivity (Fig. 2). The dry UCNP powder was found to adhere well to fingerprints. A clear-cut green luminescent image of an LFP without background fluorescence interference could be obtained under 980 nm laser excitation. Kumar et al. [28] have also synthesized a La_2O_3:Er^{3+}/Yb^{3+} phosphor powder with uniform particle morphology for background-free LFP imaging.

Compared to their bulk counterpart, UCNPs show less efficient upconversion luminescence owing to their small size. Meanwhile, UCNPs possess low two-photon absorption cross-sections, which also influence their luminescent efficiency; accordingly, a pulsed laser with high excitation power density is often required in imaging with UCNPs [29]. To solve these problems, Song et al. [29] have prepared semiconductor plasmon nanoparticle-modulated core–shell nanocomposites,

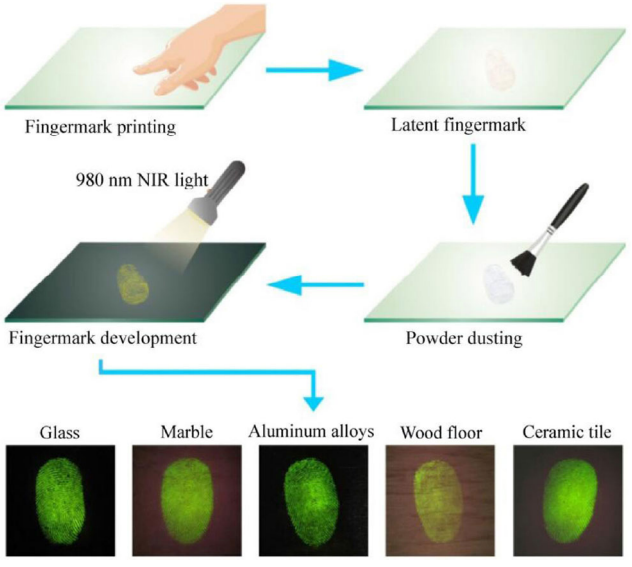

Figure 2 Schematic illustration of visualizing the LFPs by means of a UCNP powder dusting process and the fluorescent images of LFPs on various surfaces. Reproduced with permission from Ref. [27], © Tsinghua University Press and Springer-Verlag Berlin Heidelberg 2015.

referred to as $m$$Cu_{2-x}S@SiO_2@Y_2O_3$:$Yb^{3+}$/$Er^{3+}$. Because both the excitation field and the resonance energy transfer rate from Yb^{3+} ions to Er^{3+} ions increased, a 30-fold upconversion enhancement was obtained. The nanocomposites were then applied to LFP imaging. The resultant LFP image is hardly affected by background fluorescence interference, thus providing excellent optical contrast. In addition, owing to the excitation power-dependent optical property, the fluorescent color of the LFP images could be modulated from green to orange. Furthermore, Song et al. [30] have successfully constructed a plasmon-enhanced upconversion device, and high-resolution detection of LFPs was achieved with the device.

3 LFP imaging based on different emission wavelengths

In LFP imaging, if the emission wavelengths of the contrast agents and the background chromophores are different, the detection signal can be distinguished from the background signal with the assistance of color filters, resulting in improvement of the sensitivity and resolution of LFP imaging. Accordingly, it is feasible to choose an imaging agent that has an emission

wavelength different from that of the background chromophores to eliminate the background fluorescence interference. In this section, we provide a comprehensive review of contrast agents with the emission wavelength different from that of the background chromophores for background-free LFP imaging.

3.1 Organic dyes

As we mentioned above, amino acids are key components that are derived from skin secretions for the LFP generation [6]. Many organic dyes targeting amino acids have been developed for LFP imaging. Ninhydrin is the first amino acid-sensitive agent that reacts with amino acids to yield a new blue-purple color known as Ruhemann's purple [32, 33]. Later, a variety of fluorescent ninhydrin analogues such as 1,8-diazafluoren-9-one (DFO) and 1,2-indanedione (IND) have been developed and tested for LFP imaging [34, 35]. Compared to ninhydrin, DFO reacts with amino acids to give a highly fluorescent and colorimetric detection of LFPs. The fluorescent images of LFPs can be clearly visualized with a 503–587 nm excitation filter and a 593 nm viewing long pass filter [34]. IND has a similar dual mode detection function, except with the excitation wavelength of 505 nm and a 550 nm barrier filter [35]. Some natural products, such as genipin and lawsone, extracted from the gardenia fruit, also work well in background-free LFP imaging [36, 37]. The fluorescent impressions of LFPs can be further enhanced by treatment with zinc and cadmium salts [32, 35]. In addition, some other amine-sensitive agents, such as p-dimethylaminobenzaldehyde (DMAB) and p-dimethylaminocinnamaldehyde (DMAC), have been successfully applied to LFP imaging [38].

Proteins too can serve as the targets for LFP imaging. Maynard et al. [39] have achieved visualization of LFP using a lysozyme aptamer-based contrast agent. Because aptamers were modified with a fluorescent tag, fluorescent images of LFPs can be obtained under the excitation with 505 nm coupled to a camera fitted with a 555 nm bandpass filter. Highly defined level 1 and 2 features are clearly observed. The design takes advantage of the good performance and easy operation of aptamer-based contrast agents. More importantly, aptamers are introduced into the field of LFP imaging for the first time, and this pioneering design opens a new avenue for LFP imaging with high selectivity and sensitivity. Owing to changes in the type of aptamer, aptamer-based contrast agents are capable of targeting a wealth of fingerprint components, thus providing an enormous potential for practical applications.

In addition to amino acids, some water-insoluble substances, such as lipids and triglycerides, are other main components of an LFP impression [7]. Contrast agents that can target these water-insoluble components via hydrophobic interaction are also largely used in fingerprint imaging. Because of its preferential binding to lipids, Nile red can be applied to LFP imaging with colored and fluorescent prints. On the other hand, the poor solubility of Nile red limits its further applications. Recently, Lewis et al. [40] reported that Nile blue A can be employed for LFP imaging. After preparation in aqueous solutions, the spontaneous hydrolysis of Nile blue A can yield trace amounts of Nile red. The coexistence of two dyes in the same solution endows Nile blue A with dual staining capabilities: Nile blue A reacts with acidic fractions, such as phospholipids, to form a dark blue print, whereas Nile red instead dissolves preferentially in neutral lipids to give a pink or red impression. The photoluminescence property of Nile blue A originates from the Nile red moiety. Strong photoluminescence of LFPs was observed at an excitation wavelength of 505 nm with viewing through a 550 nm barrier filter. Even though the LFPs treated with Nile blue A show very pale blue-purple impressions on a blue background, the photoluminescent image of LFPs is very sharp and complete (Fig. 3). Miskelly et al. [41] have proposed a bodipy-based lipid selective dye, named LD540, and investigated its potential application in LFP detection. An enhanced contrast fluorescent image of sebaceous fingermarks can be obtained after the treatment with LD540.

What is more, there are some fantastic compounds that can mainly bind to sebum within the ridges of LFPs [42, 43]. These molecules, mainly silole compounds and silole analogues, are nonluminescent in the soluble state but will emit enhanced luminescence after aggregation. This interesting phenomenon is defined as "aggregation-induced emission (AIE)". AIE is related to the restriction of intramolecular rotations of chromophoric molecules in an aggregate state [44].

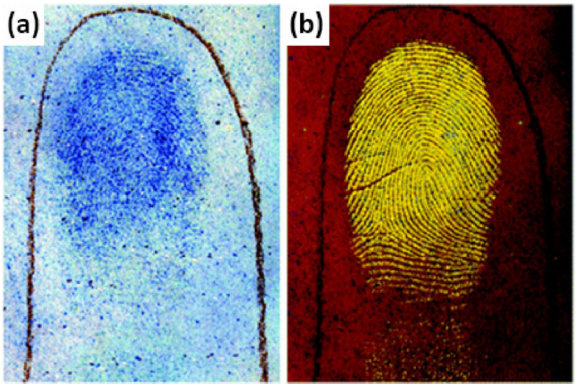

Figure 3 Latent fingerprints on white copy paper treated with Nile blue A. A representative photograph of LFPs under white light (a) and in photoluminescence mode with excitation wavelength at 505 nm and a 550 nm barrier filter (b). Reproduced with permission from Ref. [40], © The Royal Society of Chemistry 2014.

The enhanced binding affinity between the AIE molecules and residues of LFPs facilitates the aggregation of AIE molecules and the luminescence will be improved, thus leading to a reduction in background fluorescence interference. There have been some reports about LFP imaging based on the AIE effect [43, 45–47]. Su et al. [42] have reported LFP imaging based on the AIE effect of tetraphenylethene (TPE) in 2012. TPE preferentially aggregated on the ridges of LFP through hydrophobic interactions and the aggregates emitted strongly under UV illumination, thereby offering sufficient optical contrast against the background. Later, Su et al. [45] prepared several AIE compounds with different substituents—TEP, 1,1,2,3,4,5-hexaphenylsilole (HPS), and 1-methyl-1-(4-carboxystyrene)-2,3,4,5-tetraphenylsil-ole (MCSTPS)—and explored their LFP imaging performance. Very recently, Iyer et al. [47] prepared an AIE-active conjugated polyelectrolyte (CPE), named PFTPEBT-MI, and implemented quick LFP imaging with high sensitivity, high contrast, and no background interference (Fig. 4). The amphiphilic CPE may interact strongly with LFP ridges through electrostatic and lyophilic interactions. Compared to the single hydrophobic interaction, the electrostatic interaction also contributed to the enhanced and selective binding affinity, thus reducing the background interference vis-à-vis improving the imaging contrast.

3.2 Polymer-based contrast agents

Polymer materials have attracted extensive attention

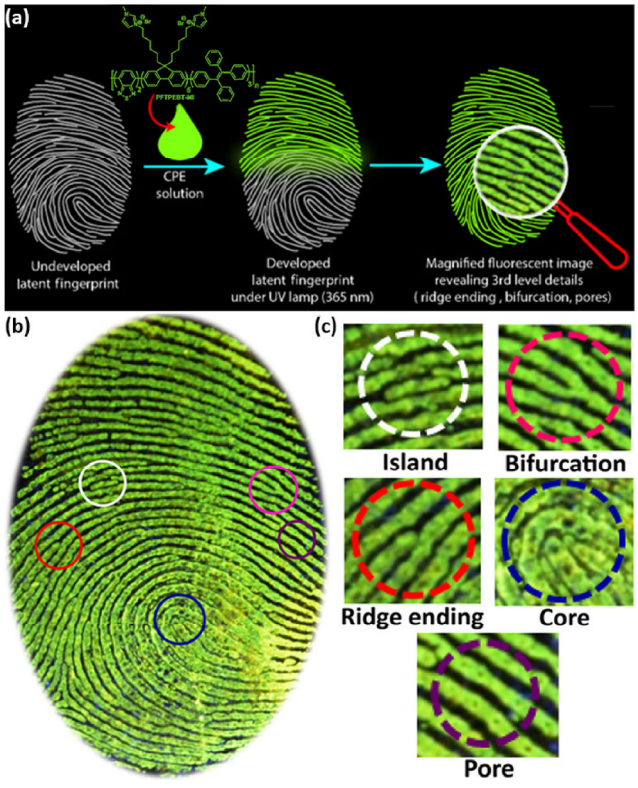

Figure 4 (a) Schematic illustration of the AIE-based LFP imaging. (b) High-resolution photographs of LFPs after developing with PFTPEBT-MI (c) showing level 1−3 details. Reproduced with permission from Ref. [47], © American Chemical Society 2017.

owing to their abundant and customized properties. Introduction of various functional side groups, such as a fluorescent moiety or a photosensitizer, into monomers may endow a polymer with a completely new property [48]. Cyanoacrylate ethyl ester, which can polymerize and cure rapidly in the presence of nucleophiles, has been employed in LFP detection for a long time [31, 49]. When a fingerprint is treated by monomer vapors in a closed chamber, the eccrine and sebaceous components within the fingerprint induce polymerization of the monomer to form a white impression. Nonetheless, the developed fingerprints sometimes are only slightly visible because of the white color. Instead, the monomer modified with a fluorescent side group has been found to be an effective contrast agent for LFP imaging [49]. Jong-Man Kim et al. [50] have successfully developed new polydiacetylenes (PDAs) that contain hygroscopic elements in their headgroup and next constructed a hydrochromic sensor for sweat pore mapping in LFPs (Fig. 5). The blue PDAs were prepared by polymerization of

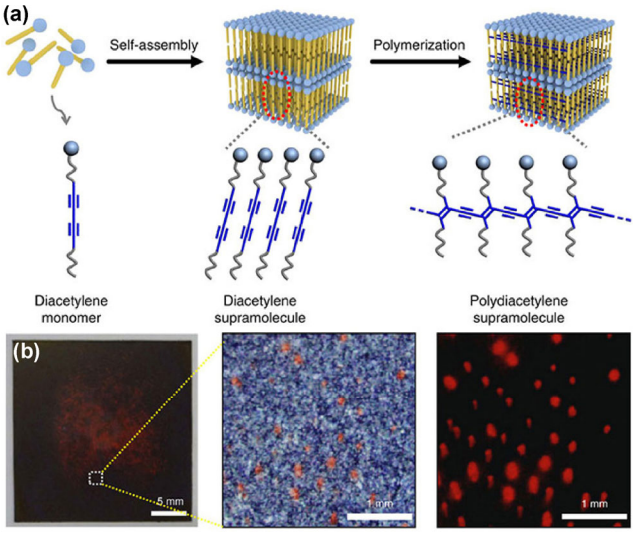

Figure 5 Hydrochromic PDAs for mapping of sweat pores. (a) Schematic illustration of fabrication of the PDAs. (b) A photograph of a fingerprint image (left) printed on a PDA film and the corresponding optical (middle) and fluorescence (right) microscopy images of the magnified fingerprint area marked in the fingerprint image. Reproduced with permission from Ref. [50], © Nature Publishing Group 2014.

self-assembled diacetylene monomers under UV irradiation. Due to the presence of the hygroscopic elements, PDAs may undergo a blue-to-red color transition upon exposure to water. Besides, PDAs afford a significant fluorescence enhancement in the presence of water. Exocrine sweat glands are distributed in higher density in fingers, and eccrine sweat contains a large amount of water. Sweat pores that serve as the "door" of the exocrine glands belong to the level 3 features of LFPs. Previous studies have indicated that 20–40 sweat pores are sufficient to generate patterns that are required for individual identity [51]. As shown in Fig. 5(b), the formation of red dots under an optical microscope and the obvious emitting dots under a fluorescence microscope indicated that the hydrochromic mapping of human sweat pores was successfully achieved. The sensor was next successfully subjected to further reliability testing and a test of active sweat pores. The strategy opens up a new way of LFP imaging via locating sweat pores.

Kwak et al. [52] have reported a lipid-responsive fluorescent conjugated polymer film of poly[1-phenyl-2-(p-trimethylsilyl)phenylacetylene] (PTMSDPA) for LFP imaging. When a finger touched the PTMSDPA film, the lipid fractions would move into the polymer film, resulting in a significant fluorescence enhancement owing to the process named swelling-induced emission enhancement. Under excitation, high-resolution and contrast-enhanced LFP images were obtained. Moreover, Wu et al. [53] have reported a novel method for detection of LFPs by means of oxetane-functionalized semiconductor polymer dots (Ox-Pdots) as a fluorescent labeling marker and an LFP preservation agent. Because of the photo-cross-linking of oxetane aided with a photoinitiator under UV excitation, a three-dimensional (3D) intermolecular polymer network was formed. The resultant LFP pattern showed unparalleled stability compared with the conventional Pdots, and the preservation time was obviously prolonged, allowing for long-term analysis of LFPs. Other research groups also reported polymer-based contrast agents for LFP imaging [54–56].

The above studies are about the LFP detection based on single polymer materials. The following examples are about polymer composite-based LFP imaging. The formation of hybrid materials can combine the advantages of different materials, and the performance of the hybrid materials cannot be achieved with any single component. For instance, Jong-Man Kim et al. [57] have fabricated diacetylene (DA)-magnetite composites and tested their capacity for imaging of sebaceous LFPs. The composites combine the advantages of two individual components, such as a stimulus-responsive color, fluorescence changes, and a magnetically responsive property. The prepared polymer composite powder manifested enhanced affinity for the sebaceous ridges when a magnetic field was applied, thus improving the LFP imaging contrast. Besides, the monomer may undergo a pale brown-to-blue color transition upon UV irradiation, and further heat treatment of the LFP image produces a red and fluorescent LFP. A suitable arrangement of the three-color property coupled with the fluorescence property was successfully employed to realize efficient visualization of LFPs deposited on pieces of paper with different background colors. Other research groups have also reported fluorescent polymer composites, such as surfactant-containing conjugated-polyelectrolyte colloidal solutions and a fluorescent dye–polymer composite film for LFP detection [58–62]. Such materials offer an effective platform for sensitive LFP imaging

and fingerprint analysis.

3.3 Inorganic nanoparticles

These nanoparticles have been developed as an important contrast agent due to their charming physicochemical properties, such as controlled synthesis, diverse morphology, fine-tuned optical properties, and excellent stability [63]. Additionally, the large surface area of inorganic nanoparticles provides abundant binding sites for various functional molecules for recognizing the targets within LFPs; therefore, inorganic nanoparticles serve as candidates for LFP imaging [64]. Several kinds of inorganic nanoparticles that have been widely used in background-free LFP imaging will be discussed in this section.

3.3.1 QDs

Since the first report about CdS semiconductor QD-based detection of LFPs reported by Menzel et al. in 2000 [65], various QD systems have been developed for imaging applications [66–72]. Owing to their excellent optical performance, such as good photostability, a high quantum yield, and size-tunable fluorescent colors, QDs provide a suitable tool for LFP imaging with high sensitivity and high contrast against the background. Moreover, the possibility of simultaneous excitation of multiple QDs by a single light source also facilitates the development of multicolor imaging. Wu et al. [66] have used Mn-doped ZnS QDs capped with N-acetyl-cysteine for the detection of LFPs in 5 s. The fast imaging benefits from the hydrophobic and electrostatic interactions between N-acetyl-cysteine and the secretions from eccrine. Because QDs have high brightness, sufficient contrast against the background could be obtained under UV excitation. Zhang et al. [67] have synthesized CdTe-montmorillonite (CdTe-MMT) nanocomposites and investigated their capacity for enhanced detection of LFPs. Given that QDs are confined to the layered structure of the sodium MMT matrix, the prepared nanocomposites show enhanced chemical stability in the air and tunable photoluminescence, thus being an alternative fluorescent labeling marker for LFP imaging. The ridge details of LFPs treated with the QD nanocomposites could be clearly visualized without obvious background staining under UV illumination.

More recently, carbon quantum dots (CQDs) have attracted considerable interest owing to their excellent photoluminescent performance [73, 74]. Unlike conventional Cd-doped QDs, CQDs, a kind of carbon nanomaterials, are biocompatible and nontoxic to humans [75]. Wang et al. [73] have prepared water-soluble CQD-based fluorescent ink for LFP imaging. Upon applying the CQDs ink, a clear-cut, permanent, and high-contrast LFP image without background fluorescence was formed on commercially available filter paper. Kelarakis et al. [14] have reported for the first time the application of CQD-based powders to LFP enhancement. The hybrid powders that contain a low concentration of CQDs, yielded excitation wavelength-dependent emission color. Specifically, the hybrid powders appeared to be blue, green, or red when they were excited in the violet, blue, and green wavelength regions, respectively. Therefore, these powders provided significant advantages for overcoming the background fluorescence interference after simple selection of a suitable fluorescent color. Besides, other research groups reported a series of CQD-based imaging agents and explored their color-tunable characteristics for LFP imaging [74–76].

The above-mentioned QD-based imaging agents have such features as a single-excitation, single-emission fluorescent mode. The following studies focus on the single-excitation, dual-emission QD hybrid materials [77, 78]. Compared with these single-excitation, single-emission fluorescent materials, dual emission QDs can not only realize LFP imaging on various colored or fluorescent surfaces (after a suitable emission wavelength is chosen) but also can be applied to the analysis of multiple LFP components. Xu et al. [77] have developed a dual-emitting QD nanohybrid for simultaneous LFP imaging and TNT visualization (Fig. 6). Specifically, polyallylamine (PAM)-modified green QDs and red QD-doped silica nanoparticles were assembled into a core–shell nanohybrid with the dual-emitting fluorescence property. Because of the formation of a Meisenheimer complex between the primary amines of PAM and TNT, the green-emitting QDs may be quenched by TNT while the red one remains unchanged. Therefore, the nanohybrid manifested tunable visible multicolor fluorescence because of TNT-modulating Förster resonance energy

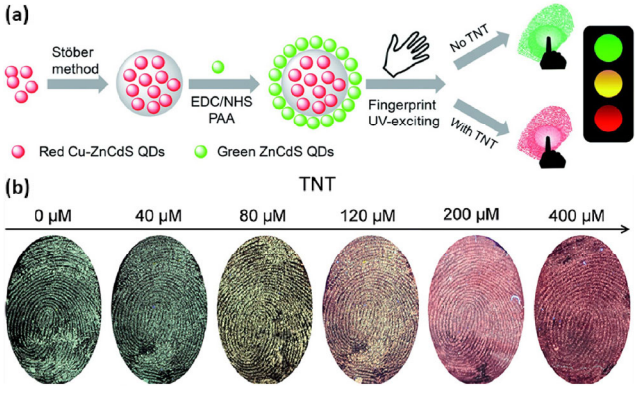

Figure 6 (a) Schematic illustration of preparation of the nanohybrid of green/red QDs for simultaneous LFP imaging and visualization of TNT. (b) Fluorescence images of LFPs with increasing amounts of TNT. Acquisition of all fluorescence images involved excitation with a 365 nm UV lamp. Reproduced with permission from Ref. [77], © The Royal Society of Chemistry 2015.

transfer under UV illumination. This method can promote the application of QD-based contrast agents in security screening.

3.3.2 *Lanthanide-doped luminescent nanomaterials*

Lanthanides represents a group of rare elements that constitute the 5d block of the periodic table and possess abundant electronic levels. The unique electronic configuration gives lanthanides interesting and attractive optical properties. Due to the presence of electron-filled $5s^25p^2$ subshells that can protect the inner 4f orbital from environmental interference, the energy of different electronic levels included in 4f orbitals is well-defined and the 4f–4f electronic transitions are inert to the chemical environment around lanthanide materials. Consequently, lanthanide ions are characterized by characteristic and sharp emission patterns that fall in the range of visible and NIR region [79]. Lanthanide-doped fluorescent materials possess the advantages of high photostability and high fluorescence intensity, enabling them to be an ideal fluorescent label for background-free LFP imaging [80, 81].

Mao et al. [80] have reported two kinds of lanthanide-doped nanomaterial for LFP imaging: red-emitting YVO_4:Eu nanocrystals and green-emitting $LaPO_4$:Ce,Tb nanobelts. The small size and high luminescence intensity enable high contrast and low background interference in LFP imaging. As illustrated in Fig. 7,

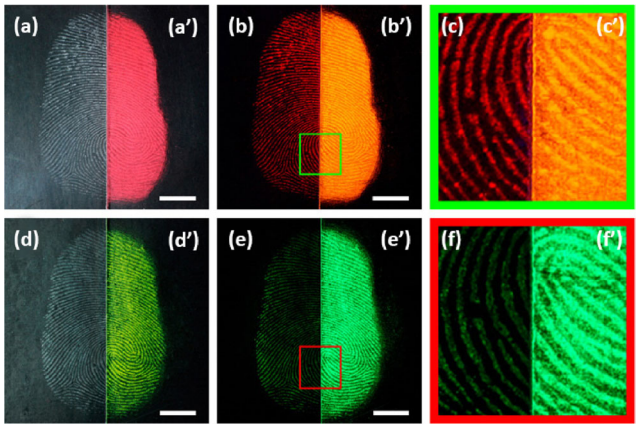

Figure 7 LFPs treated with (a)–(c) red fluorescent YVO_4:Eu nanocrystals and (d)–(f) green fluorescent $LaPO_4$:Ce,Tb nanobelts as well as (a')–(c') conventional red and (d')–(f') fluorescent powders. (a), (a'), (d), and (d') Optical images in a bright field, (b), (b'), (e), and (e') fluorescence images in a dark field under 254 nm UV irradiation. (c), (c'), (f), and (f') Magnified images of the small box in (b), (b'), (e), and (e'). The scale bar is 5.0 mm. Reproduced with permission from Ref. [80], © American Chemical Society 2015.

compared with conventional red and green fluorescent powders, the resultant LFP image obtained by means of the two lanthanide-doped luminescent nanomaterials exhibited high quality fluorescent impression under UV irradiation. Shi et al. [81] have synthesized two types of lanthanide-doped tetragonal phase t-$LaVO_4$ nanoparticles, both with excellent luminescent properties. In particular, the Eu^{3+}-doped t-$LaVO_4$ emitted bright red light, and Eu^{3+}-doped t-$LaVO_4$ emitted yellowish light close to white under UV illumination. After treatment with the lanthanide-doped nanomaterials, the developed luminescent LFPs could be viewed clearly under UV light. On account of their high luminescence intensity, the luminescent LFPs developed on various surfaces afforded high contrast against background interference. Impressively, the second-level detail information, such as breaks and bifurcations, could be obtained from the corresponding magnified images.

3.3.3 *Transition metal-doped luminescent nanomaterials*

The IUPAC defines a transition metal as "an element whose atom has a partially filled d sub-shell, or which can give rise to cations with an incomplete d sub-shell". Due to their particular electronic configuration, transition metal ions can serve for doping various materials to bring about fantastic properties [82, 83].

Recently, our group [84] successfully prepared Mn-and-Ga-codoped Zn_2GeO_4 nanoparticles for background-free LFP imaging. The nanoparticles show bright green emission under UV excitation. LFP imaging was conducted on a hardboard with strong blue background fluorescence. As shown in Fig. 8(a), the LFP images are deeply buried in the blue background fluorescence under UV illumination. By contrast, as shown in Fig. 8(b), upon application of the 510 nm long pass filter, the background fluorescence was effectively removed, and a sharp LFP image with a well-defined ridge pattern was obtained. These results clearly indicate that the development of contrast agents with an emission wavelength different from that of the background chromophores can serve as an effective way to avoid background fluorescence.

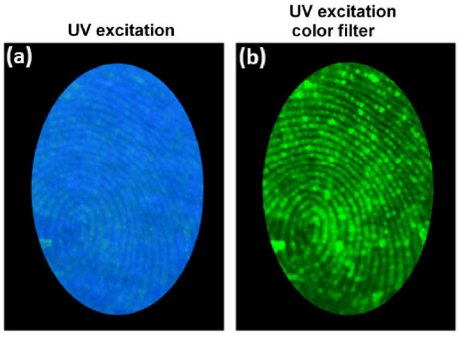

Figure 8 Luminescent images of LFPs under UV excitation obtained without (a) and with (b) optical filtering (510 nm long pass filter). Reproduced with permission from Ref. [84], © American Chemical Society 2017.

3.3.4 *Luminescent metal nanoclusters*

Noble-metal clusters made of a few tens of atoms with size < 2 nm possess unique physical and chemical properties [85]. Ag nanoclusters (AgNCs), some of the representative metal clusters, have unique fluorescent properties that can readily be modulated by changing the surrounding microenvironments [86]. On the basis of this interesting optical property, Qu et al. [87] have provided a versatile and simple approach for the detection and visualization of LFPs by combining the DNA-programmed AgNCs and DNA aptamers (Fig. 9). Specifically, a G-rich region was designed at the end of the lysozyme-binding aptamers. The DNA template AgNCs can be hybridized with the designed aptamers. Because the emission pattern of the AgNCs is sensitive to the nearby DNA region, the hybridization can alter the microenvironment around AgNCs, thus leading to bright red emission. Similarly, green-emitting AgNCs that can target TNT were also successfully prepared. After treatment of LFPs with the two lightened-up AgNCs, multicolor LFP imaging and simultaneous identification of lysozyme and TNT were implemented. More importantly, quantitative detection of fingerprint components was also accomplished. The strategy holds an enormous potential for LFP identification and further practical application.

3.3.5 *Dye-labeled nanomaterials*

Noble metal nanoparticles [64, 88–93] and metal oxide

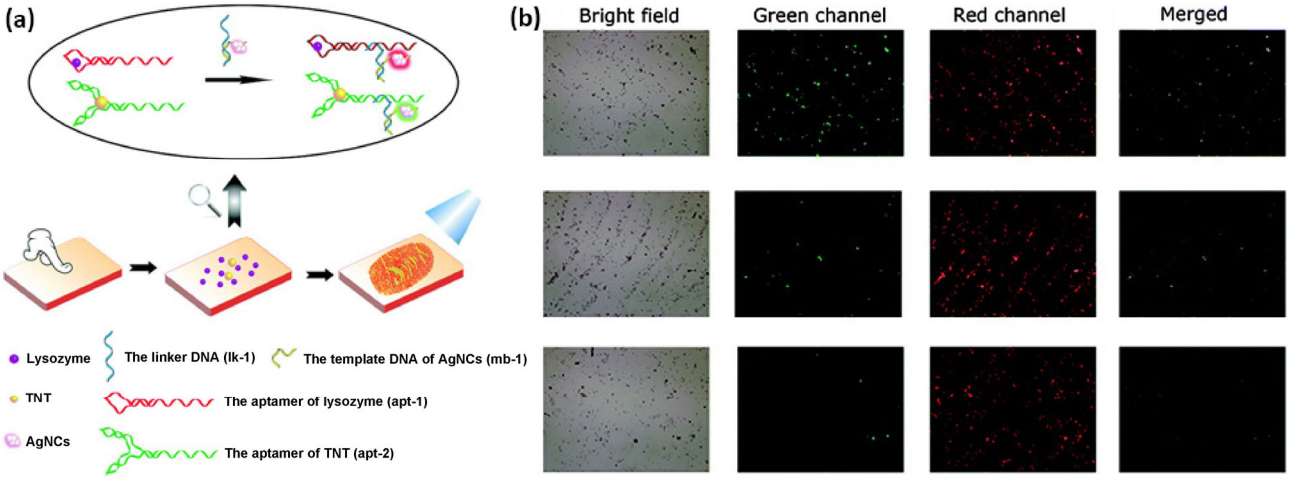

Figure 9 (a) Schematic illustration of visualizing the LFPs using DNA-regulated AgNCs. (b) Higher magnification bright-field and fluorescence images of LFPs with increased concentrations of TNT from the bottom row to the top. Reproduced with permission from Ref. [87], © The Royal Society of Chemistry 2016.

nanoparticles [94–98], which are two widely used contrast agents for LFP imaging, can be modified with an antibody to realize immunolabeling imaging. Indeed, metal nanoparticles have been applied to LFP imaging for a long time, e.g., via multimetal deposition [88, 89] and immunological multimetal deposition [90]. The immunolabeling and fluorescent imaging methods open up new opportunities for LFP imaging, detailed analysis, and even component profiling of LFPs [91, 92]. Dermcidin, which is particularly critical for the protection of skin, is one of the most abundant antimicrobial peptides in eccrine sweat [91]. Van Dam et al. [92] have used an anti-dermcidin antibody and a fluorescent dye-tagged secondary antibody for the dermcidin imaging in LFPs. This immunolabeling strategy provides a suitable tool both for LFP imaging with improved quality and detection of specific components, and also helps with access to high-level features of fingerprints. Later, Russell et al. [64] prepared gold nanoparticles (Au NPs) modified with an anti-cotinine antibody for simultaneous identification of cotinine and individuals. The large surface area of Au NPs provides abundant binding sites for the anti-cotinine antibody, and the amount of fluorescently tagged secondary antibody is increased, thus improving the fluorescence signals. After treatment with the anti-cotinine antibody-modified Au NPs, a sharp LFP image was obtained and even sweat pores could be observed. Meanwhile, cotinine in LFPs could be successfully detected too. The method provides a novel insight into the applications to illicit-drug detection and medical diagnostics.

Compared to Au NPs, magnetic nanoparticles can be directed by a magnetic field. Therefore, extra magnetic nanoparticles that fail to adhere to the LFPs can be totally removed under the influence of a magnetic field, thus enabling higher sensitivity and enhanced contrast. Russell et al. [94] have reported a simple and versatile detection platform for various drugs and drug metabolites in LFPs from drug users, such as Δ^9-tetrahydrocannabinol (THC), methadone, 2-ethylidene-1,5-dimethyl-3,3,-diphenylpyrrolidine (EDDP), and benzoylecgonine. This approach enables simultaneous individual identification and extraction of information on drug usage. Furthermore, Russell et al. [95] have successfully realized multiplexed detection of metabolites of heroin (morphine) and a metabolite of cocaine (benzoylecgonine) in LFPs (Fig. 10). Magnetic nanoparticles were modified with an anti-morphine antibody and anti-benzoylecgonine antibody, separately. The two kinds of nanoparticles were incubated over two separate sections of fingerprints. After removal of excess particles using a magnet, an Alexa 488-labeled secondary antibody and an Alexa

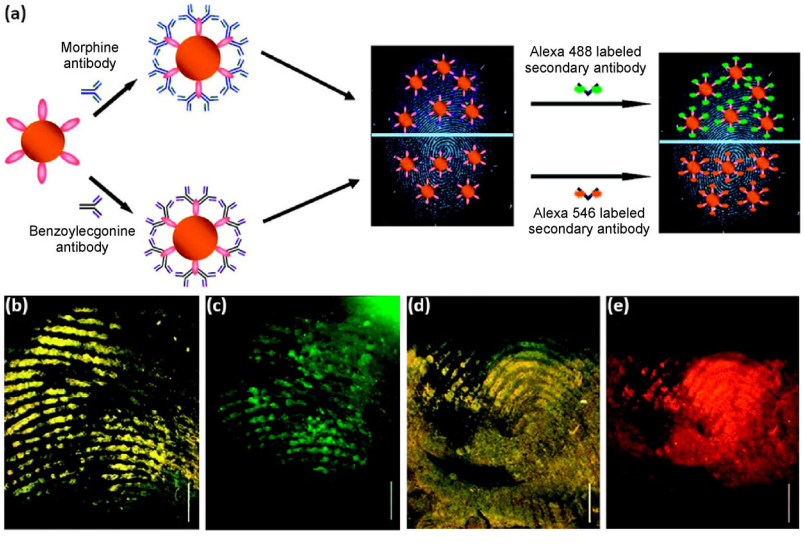

Figure 10 (a) Schematic illustration of the detection of two drug metabolites from a single fingerprint via antibody–magnetic particle conjugates. (b) Bright-field and (b) fluorescence images of the upper portion of a fingerprint used for the detection of morphine. (d) Bright-field and (e) fluorescence images of the lower portion of the fingerprint used for the detection of benzoylecgonine. The scale bar is 2.0 mm. Reproduced with permission from Ref. [95], © American Chemical Society 2010.

546-labeled one were employed to treat the two above-mentioned sections, respectively. A dual-color image of LFPs with high quality and high resolution could be obtained by bright-field and fluorescence microscopy, enabling simultaneous individual identification and extraction of information on drug usage.

4 LFP imaging based on different luminescence lifetime values

Inspired by the short-lived background fluorescence, the following notion has been proposed: If the signals of contrast agents are collected after the background fluorescence disappears, the background fluorescence interference can be totally removed [99]. Since the discovery of $SrAl_2O_4$:Eu/Dy with bright persistent luminescence in 1996, persistent phosphors have attracted significant attention owing to their unique optical properties [100–102]. Persistent phosphors can remain luminescent after the removal of excitation, thus serving as another ideal candidate for background fluorescence-free imaging.

Our group has conducted several studies on controlled synthesis and exploring of biomedical applications of persistent-luminescence nanoparticles (PLNPs) [84, 103–106]. In one of our studies [84], we have proposed a PLNP-based time-gated imaging method for background-free LFP imaging and visualization of protein secretions (Fig. 11). Specifically, we successfully synthesized Zn_2GeO_4:1.0%Ga,0.5%Mn (ZGO:Ga,Mn) nanoparticles via the "bottom up" approach, and the decay time of luminescence in ZGO:Ga,Mn nanoparticles exceeded 20 min. After modification of carboxyl groups followed by treatment with EDC/NHS, active esters on the surface of ZGO:Ga,Mn nanoparticles were formed. Because of the reaction between the active esters and the abundant intrinsic amino group in the ridges, the ZGO:Ga,Mn PLNPs could be linked to the LFPs covalently. The as-treated LFPs were activated with a portable UV lamp for a while. After removal of the UV lamp, the background fluorescence faded rapidly, and a green LFP image was obtained because ZGO:Ga,Mn PLNPs remained luminescent. Furthermore, after functionalization with concanavalin A (ConA), which can specifically recognize glycoproteins, the ZGO:Ga,Mn persistent nanoparticles were successfully applied to the imaging of glycoproteins in LFPs. The strategy provides a versatile platform both for background-free LFP imaging and specific visualization of fingerprint components, thus being valuable for forensic investigations and medical diagnostics.

5 LFP imaging based on different plasmonic properties

The free electron gas of noble metal nanoparticles may produce resonant oscillation, named localized surface plasmon resonance (LSPR) upon stimulation by an incident light whose wavelength is greater than the nanoparticle [107]. The resonant frequency is dependent on the nanoparticles' size, shape, and

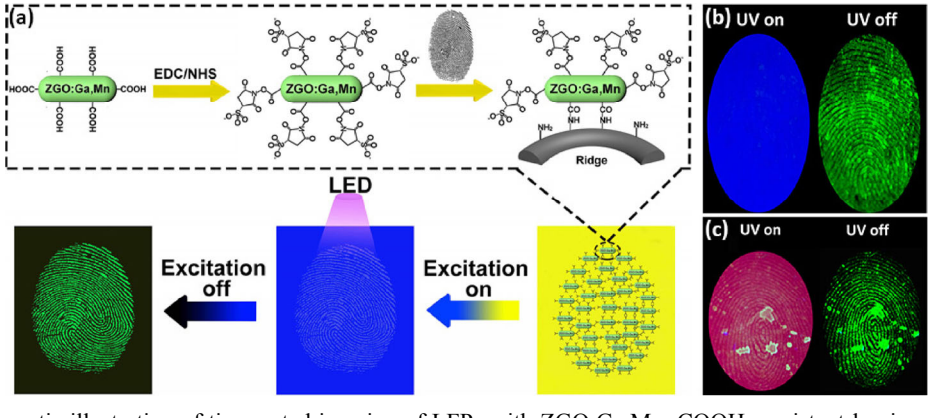

Figure 11 (a) Schematic illustration of time-gated imaging of LFPs with ZGO:Ga,Mn−COOH persistent-luminescence nanoparticles. A photograph of a treated fingerprint on a poker card (b) and a soft drink can (c) under UV excitation and after excitation ceases. Reproduced with permission from Ref. [84], © American Chemical Society 2017.

composition [108]. Because of the presence of LSPR, these nanoparticles can absorb and scatter intense light that can be directly observed visually with the aid of dark-field microscopy (DFM) [107]. Among the various noble metal nanoparticles, gold and silver are the most widely used materials, especially Au NPs. In these above-mentioned Au-based imaging methods, Au NPs serve only as "glue" that adheres to LFPs and as "carriers" of signaling and recognition molecules. The LSPR properties of Au NPs are not used [109]. In this section, colorimetric imaging, plasmonic imaging, and photoacoustic imaging based on Au NPs will be introduced.

Aggregation of Au NPs leads to a shift of the LSPR band, and an obvious color change will occur [110]. Thus, LFP residue-induced aggregation of Au NPs can be applied to colorimetric detection of LFPs [111]. Additionally, an obvious change of a scattering signal also can be detected by DFM. In this regard, Li et al. [109, 112] have done excellent work on the nanoplasmonic imaging of LFPs. They [109] have used cocaine aptamer-modified Au NPs for the LFP imaging and cocaine visualization (Fig. 12). Specifically, two types of Au NPs were modified with a split of cocaine-specific aptamer. In the presence of cocaine, the two splits of cocaine aptamer can direct Au NPs to aggregate, resulting in green-to-red color change of the scattered light in the DFM images. Because few background compounds in the underlying substrates possess plasmonic properties, this method can efficiently eliminate background interference such as a background color or background fluorescence. As shown in Fig. 12(b), the level 2 and level 3 features of the LFPs can be clearly observed. Moreover, quasi-quantitative cocaine detection is realized. This strategy holds enormous promise both for LFP imaging and analysis of any small molecules or proteins in LFPs.

Except for the nanoplasmonic imaging, the presence of the LSPR effect also makes Au NPs tunable and gives them strong optical absorption; subsequently, Au NPs can release the absorbed energy in the form of an acoustic wave [113]. Hence, Au NPs can serve as PA contrast agents for photoacoustic (PA) imaging. The scattering of ultrasonic signals is much weaker than that of light; thus, PA imaging manifests little background interference and provides high signal contrast. Nie et al. [111] have synthesized amphiphilic block copolymer (BCP)-capped Au NPs and realized simultaneous photoacoustic and colorimetric visualization of LFPs. When an LFP was immersed into the solution containing BCP-functionalized Au NPs, both electrostatic and hydrophobic interactions between the BCP and natural secretions (such as proteins)

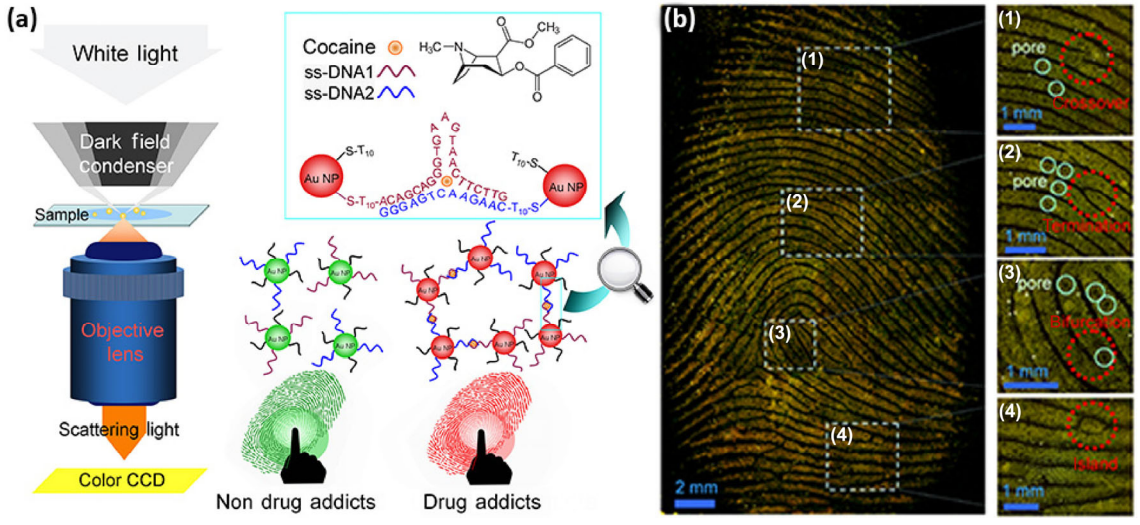

Figure 12 (a) Schematic illustration of nanoplasmonic imaging of LFPs and identification of cocaine in LFPs by DFM. (b) A dark-field image of a representative sebaceous LFP and the level 2 details including crossover (1), termination (2), bifurcation (3), and island (4) as well as level 3 details (pores in (1), (2), (3), and (4)). Reproduced with permission from Ref. [109], © American Chemical Society 2017.

facilitated the aggregation of Au NPs on the LFP residues. The resultant color of LFP could be tuned by controlling the self-assembly behavior. Moreover, in PA imaging mode, a clear-cut LFP with high resolution and high contrast could be obtained, allowing for observation of level 3 hyperfine features of LFPs.

Moreover, the phenomenon of surface-enhanced Raman scattering (SERS) is closely related to LSPR owing to their complementary nature [108]. When the LSPR of noble metal nanoparticles is coupled with Raman excitation and emission, the electromagnetic enhancement in SERS can be achieved, thus resulting in an increased SERS signal. SERS analysis has such features as high sensitivity, providing an additional approach for detection of secretions within LFPs. In this regard, some research groups have developed an Ag NP-enhanced Raman technique for visualization of LFP and SERS analysis of various endogenous and exogenous components in LFPs [114–118].

6 LFP imaging based on different photothermal properties

As the name implies, the photothermal phenomenon represents the conversion of electromagnetic irradiation to heat [108]. In contrast to optical imaging, photothermal imaging provides an additional means of eliminating background interference because of its distinctive detection signal. Wang et al. [119] have prepared hydrophobic Cu_7S_4 semiconductor nanoparticles. The nanoparticles were further modified with allyl mercaptan and then used to fabricate amphiphilic nanocomposites (NCs) via polymerization of allyl mercaptan to ensure good binding affinity for LFP residues. The resultant NCs showed good performance in the detection of LFPs deposited on various colored substrates (Fig. 13). What is more, amine group-rich bifunctional nanocomposites contained Cu_7S_4 nanoparticles, and CdSe@ZnS QDs were also fabricated. Owing to the formation of a Meisenheimer complex between an amine group and TNT, the fluorescence of QDs may be quenched while the photothermal ability is unaffected. Hence the dual-mode imaging for simultaneous visualization of LFPs and TNT residues could be implemented. The design opens up a new avenue for the use of photothermal agents for LFP imaging.

7 LFP imaging based on different electrochemiluminescence (ECL) properties

In addition to the above-mentioned various methods, ECL shows outstanding performance in LFP imaging

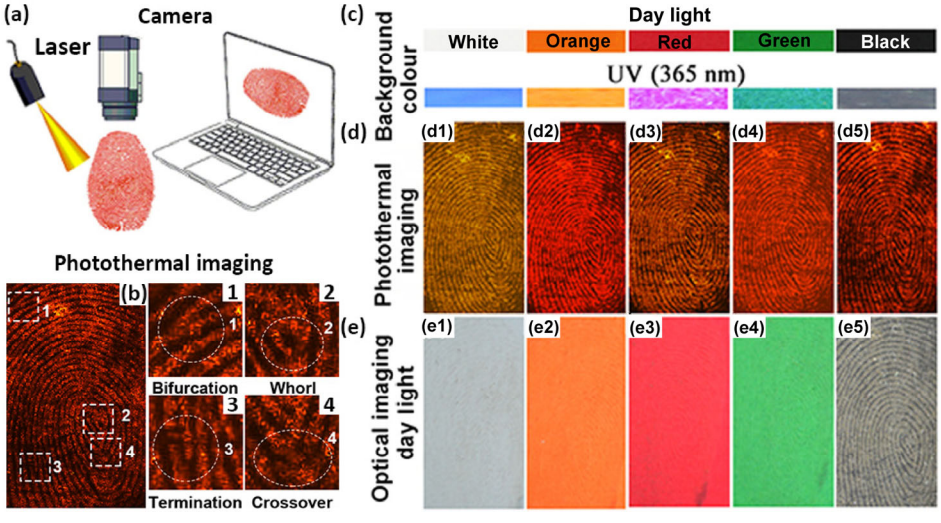

Figure 13 (a) The scheme for photothermal imaging of LFPs. (b) The photothermal imaging of LFPs and the level 2 details. (c) The illustration of different background colors under daylight and UV irradiation. (d) Photothermal images of LFPs treated with Cu_7S_4 NCs under irradiation at 808 nm. (e) Optical images of LFPs treated with Cu_7S_4 NCs under daylight. Reproduced with permission from Ref. [119], © American Chemical Society 2015.

with high sensitivity. ECL is chemiluminescence triggered by electrochemical methods, and no additional light sources are required; therefore, background signals produced by light irradiation can be efficiently avoided [120]. Because the light-emitting species are produced *in situ* close to electrode surfaces, ECL reflects only the local surface reactivity, and a near-zero background can be achieved [121]. These excellent properties no doubt pave the way for background-free LFP imaging [121–123].

Su et al. [121] have reported visualization of sebum-rich LFPs by ECL (Fig. 14). On the one hand, the presence of the sebaceous components in the ridges may decrease the electrochemical activity of the underlying electrode surface. Hence, when the electrode was exposed to a solution containing the ECL-generating luminophore, the ECL reaction and subsequent light emission could occur on the bare surface uncovered by the LFPs, resulting in a negative image of LFPs. On the other hand, because abundant amino acids were contained in LFPs, the light emission could be produced on the ridges of the LFPs when the ECL-generating luminophore was modified with an amino acid-active N-hydroxysuccinimide ester, and a positive image of LFPs was obtained. Furthermore, according to the molecular recognition between the proteins or peptides in the LFPs and their corresponding antibody, Su et al. [123] have implemented simultaneous LFP imaging and immunodetection of secretions in human perspiration via chemiluminescent oxidation of luminol by a horseradish peroxidase (HRP) molecule. It should be noted that an immunoassay involving multiple HRP molecules may increase the chemiluminescence intensity, thereby increasing detection sensitivity.

8 Conclusion and outlook

Over the past decades, advances in contrast agents and new technologies have accelerated the development of background-free LFP imaging. In this review, we summarized the recent developments in elimination of background interference with contrast agents showing optical properties different from those of the background compounds. This review will provide a guidance for researchers on selection of materials and imaging methods for not only LFP imaging but also for other imaging applications. With advancement of the LFP technology, the quantitative, multiplexed, portable, and efficient imaging methods that allow for simultaneous LFP imaging and visualization of multiple components in LFPs are needed for practical applications. The multiple-mode LFP imaging methods are worth considering for the improved accuracy of LFP imaging. Furthermore, the analysis of varied chemical information on LFPs is still at its early stage, and LFP profiling provides a novel insight into the applications to forensic investigation and *in vitro* diagnostics and thus should be paid more attention.

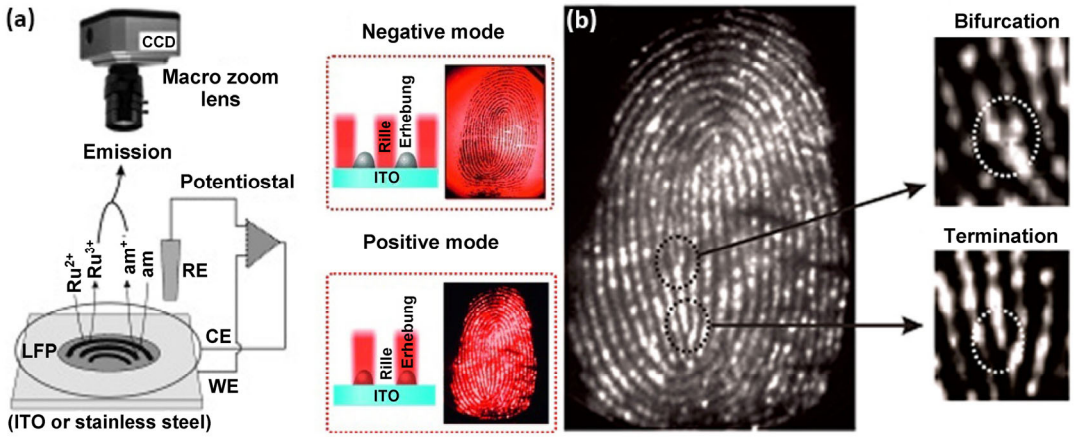

Figure 14 (a) Schematic illustration of the ECL-based detection of LFPs:Ru^{2+} and am represent the ECL-generating luminophore and the amine coreactant, respectively. (b) The ECL imaging of LFPs and the level 2 details. Reproduced with permission from Ref. [121], © John Wiley & Sons 2012.

Acknowledgements

This work was supported by the National Natural Science Foundation of China (No. 21675120), the National Key R&D Program of China (Nos. 2017YFA0208000 and 2016YFF0100800), the National Basic Research Program of China (973 Program, No. 2015CB932600) and Ten Thousand Talents Program for Young Talents.

References

[1] Hazarika, P.; Russell, D. A. Advances in fingerprint analysis. *Angew. Chem., Int. Ed.* **2012**, *51*, 3524–3531.

[2] Rastogi, P.; Pillai, K. R. A study of fingerprints in relation to gender and blood group. *J. Indian Acad. Forensic Med.* **2010**, *32*, 11–14.

[3] Wei, Q. H.; Zhang, M. Q.; Ogorevc, B.; Zhang, X. J. Recent advances in the chemical imaging of human fingermarks (a review). *Analyst* **2016**, *141*, 6172–6189.

[4] Ewing, A. V.; Kazarian, S. G. Infrared spectroscopy and spectroscopic imaging in forensic science. *Analyst* **2017**, *142*, 257–272.

[5] Bécue, A. Emerging fields in fingermark (meta)detection—A critical review. *Anal. Methods* **2016**, *8*, 7983–8003.

[6] Cadd, S.; Islam, M.; Manson, P.; Bleay, S. Fingerprint composition and aging: A literature review. *Sci. Justice* **2015**, *55*, 219–238.

[7] Comi, T. J.; Ryu, S. W.; Perry, R. H. Synchronized desorption electrospray ionization mass spectrometry imaging. *Anal. Chem.* **2016**, *88*, 1169−1175.

[8] Cortés-Salazar, F.; Momotenko, D.; Girault, H. H. Lesch, A.; Wittstock, G. Seeing big with scanning electrochemical microscopy. *Anal. Chem.* **2011**, *83*, 1493–1499.

[9] Ricci, C.; Bleay, S.; Kazarian, S. G. Spectroscopic imaging of latent fingermarks collected with the aid of a gelatin tape. *Anal. Chem.* **2007**, *79*, 5771−5776.

[10] Kelly, P. F.; King, R. S. P.; Mortimer, R. J. Fingerprint and inkjet-trace imaging using disulfur dinitride. *Chem. Commun.* **2008**, 6111–6113.

[11] Zhang, M. Q.; Becue, A.; Prudent, M.; Champod, C.; Girault, H. H. SECM imaging of MMD-enhanced latent fingermarks. *Chem. Commun.* **2007**, 3948–3950.

[12] Menzel, E. R. Recent advances in photoluminescence detection of fingerprints. *Sci. World J.* **2001**, *1*, 498−509.

[13] Chadwick, S.; Maynard, P.; Kirkbride, P.; Lennard, C.; Spindler, X.; Roux, C. Use of Styryl 11 and STaR 11 for the luminescence enhancement of cyanoacrylate developed fingermarks in the visible and near-infrared regions. *J. Forensic Sci.* **2011**, *56*, 1505−1513.

[14] Fernandes, D.; Krysmann, M. J.; Kelarakis, A. Carbon dot based nanopowders and their application for fingerprint recovery. *Chem. Commun.* **2015**, *51*, 4902–4905.

[15] Li, B.-Y.; Zhang, X.-L.; Zhang, L.-Y.; Wang, T.-T.; Li, L.; Wang, C.-G.; Su, Z.-M. NIR-responsive $NaYF_4$:Yb,Er,Gd fluorescent upconversion nanorods for the highly sensitive detection of blood fingerprints. *Dyes Pigm.* **2016**, *134*, 178–185.

[16] Wang, J.; Wei, Y. R.; Hu, X. X.; Fang, Y.-Y.; Li, X. Y.; Liu, J.; Wang, S. F.; Yuan, Q. Protein activity regulation: Inhibition by closed-loop aptamer-based structures and restoration by near-IR stimulation. *J. Am. Chem. Soc.* **2015**, *137*, 10576−10584.

[17] Yuan, Q.; Wu, Y.; Wang, J.; Lu, D. Q.; Zhao, Z. L.; Liu, T.; Zhang, X. B.; Tan, W. H. Targeted bioimaging and photodynamic therapy nanoplatform using an aptamer-guided G-quadruplex DNA carrier and near-infrared light. *Angew. Chem., Int. Ed.* **2013**, *52*, 13965–13969.

[18] Hu, X. X.; Wei, T.; Wang, J.; Liu, Z.-E.; Li, X. Y.; Zhang, B. H.; Li, Z. H.; Li, L. L.; Yuan, Q. Near-infrared-light mediated ratiometric luminescent sensor for multimode visualized assays of explosives. *Anal. Chem.* **2014**, *86*, 10484–10491.

[19] Liu, Z.-E.; Wang, J.; Li, Y.; Hu, X. X.; Yin, J. W.; Peng, Y. Q.; Li, Z. H.; Li, Y. W.; Li, B. M.; Yuan, Q. Near-infrared light manipulated chemoselective reductions enabled by an upconversional supersandwich nanostructure. *ACS Appl. Mater. Interfaces* **2015**, *7*, 19416−19423.

[20] Ma, Q. Q.; Wang, J.; Li, Z. H.; Wang, D.; Hu, X. X.; Xu, Y. S.; Yuan, Q. Near-infrared-light-mediated high-throughput information encryption based on the inkjet printing of upconversion nanoparticles. *Inorg. Chem. Front.* **2017**, *4*, 1166–1172.

[21] Tan, Y. N.; Hu, X. X.; Liu, M.; Liu, X. W.; Lv, X. B.; Li, Z. H.; Wang, J.; Yuan, Q. Simultaneous visualization and quantitation of multiple steroid hormones based on signal-amplified biosensing with duplex molecular recognition. *Chem.—Eur. J.* **2017**, *23*, 10683–10689.

[22] Zhou, J.; Liu, Q.; Feng, W.; Sun, Y.; Li, F. Y. Upconversion luminescent materials: Advances and applications. *Chem. Rev.* **2015**, *115*, 395−465.

[23] Wang, M.; Zhu, Y.; Mao, C. B. Synthesis of NIR-responsive $NaYF_4$:Yb,Er upconversion fluorescent nanoparticles using an optimized solvothermal method and their applications in enhanced development of latent fingerprints on various smooth substrates. *Langmuir* **2015**, *31*, 7084−7090.

[24] Wang, J.; Wei, T.; Li, X. Y.; Zhang, B. H.; Wang, J. X.; Huang, C.; Yuan, Q. Near-infrared-light-mediated imaging of latent fingerprints based on molecular recognition. *Angew. Chem., Int. Ed.* **2014**, *53*, 1616–1620.

[25] Wang, M. Latent fingermarks light up: Facile development of latent fingermarks using NIR-responsive upconversion fluorescent nanocrystals. *RSC Adv.* **2016**, *6*, 36264–36268.

[26] Li, J. C.; Zhu, X. J.; Xue, M.; Feng, W.; Ma, R. L.; Li, F. Y. Nd^{3+}-sensitized upconversion nanostructure as a dual-channel emitting optical probe for near infrared-to-near infrared fingerprint imaging. *Inorg. Chem.* **2016**, *55*, 10278−10283.

[27] Wang, M.; Li, M.; Yang, M. Y.; Zhang, X. M.; Yu, A. Y.; Zhu, Y.; Qiu, P. H.; Mao, C. B. NIR-induced highly sensitive detection of latent fingermarks by $NaYF_4$:Yb,Er upconversion nanoparticles in a dry powder state. *Nano Res.* **2015**, *8*, 1800–1810.

[28] Tiwari, S. P.; Kumar, K.; Rai, V. K. Latent fingermarks detection for La_2O_3:Er^{3+}/Yb^{3+} phosphor material in upconversion emission mode: A comparative study. *J. Appl. Phys.* **2015**, *118*, 183109.

[29] Zhou, D. L.; Li, D. Y.; Zhou, X. Y.; Xu, W.; Chen, X.; Liu, D. L.; Zhu, Y. S.; Song, H. W. Semiconductor plasmon induced up-conversion enhancement in $m$$Cu_{2-x}S$@$SiO_2$@$Y_2O_3$:$Yb^{3+}$/$Er^{3+}$ core−shell nanocomposites. *ACS Appl. Mater. Interfaces* **2017**, *9*, 35226−35233.

[30] Chen, X.; Xu, W.; Zhang, L. H.; Bai, X.; Cui, S. B.; Zhou, D. L.; Yin, Z.; Song, H. W.; Kim, D.-H. Large upconversion enhancement in the "Islands" Au–Ag alloy/$NaYF_4$:Yb^{3+},Tm^{3+}/Er^{3+} composite films, and fingerprint identification. *Adv. Funct. Mater.* **2015**, *25*, 5462−5471.

[31] Xie, H.-H.; Wen, Q.; Huang, H.; Sun, T.-Y.; Li, P. H.; Li, Y.; Yu, X.-F.; Wang, Q.-Q. Synthesis of bright upconversion submicrocrystals for high-contrast imaging of latent-fingerprints with cyanoacrylate fuming. *RSC Adv.* **2015**, *5*, 79525–79531.

[32] Hong, S.; Kim, M.; Yu, S. Latent fingermark development on thermal paper using 1,2-indanedione/zinc and polyvinyl-pyrrolidone. *J. Forensic Sci.* **2018**, *63*, 548–555.

[33] Brunelle, E.; Huynh, C.; Le, A. M.; Halámková, L.; Agudelo, J.; Halámek, J. New horizons for ninhydrin: Colorimetric determination of gender from fingerprints. *Anal. Chem.* **2016**, *88*, 2413−2420.

[34] Berdejo, S.; Rowe, M.; Bong, J. W. Latent fingermark development on a range of porous substrates using ninhydrin analogs—A comparison with ninhydrin and 1,8-diazofluoren. *J. Forensic Sci.* **2012**, *57*, 509−514.

[35] Patton, E. L. T.; Brown, D. H. Lewis, S. W. Detection of latent fingermarks on thermal printer paper by dry contact with 1,2-indanedione. *Anal. Methods* **2010**, *2*, 631−637.

[36] Thomas, P.; Farrugia, K. An investigation into the enhancement of fingermarks in blood on paper with genipin and lawsone. *Sci. Justice* **2013**, *53*, 315–320.

[37] Jelly, R.; Lewis, S. W.; Lennard, C.; Lim, K. F.; Almog, J. Lawsone: A novel reagent for the detection of latent fingermarks on paper surfaces. *Chem. Commun.* **2008**, 3513–3515.

[38] Fritz, P.; van Bronswijk, W.; Lewis, S. W. p-Dimethy-laminobenzaldehyde: Preliminary investigations into a novel reagent for the detection of latent fingermarks on paper surfaces. *Anal. Methods* **2013**, *5*, 3207–3215.

[39] Wood, M.; Maynard, P.; Spindler, X.; Lennard, C.; Roux, C. Visualization of latent fingermarks using an aptamer-based reagent. *Angew. Chem., Int. Ed.* **2012**, *51*, 12272–12274.

[40] Frick, A. A.; Busetti, F.; Cross, A.; Lewis, S. W. Aqueous Nile blue: A simple, versatile and safe reagent for the detection of latent fingermarks. *Chem. Commun.* **2014**, *50*, 3341–3343.

[41] Qi, A.; Miskelly, G. M. Staining using the lipid dye LD540 in fluorous media: Application to sebaceous latent fingermarks. *Anal. Methods* **2015**, *7*, 1265−1268.

[42] Li, Y.; Xu, L. R.; Su, B. Aggregation induced emission for the recognition of latent fingerprints. *Chem. Commun.* **2012**, *48*, 4109–4111.

[43] Xu, L. R.; Li, Y.; Li, S. H.; Hu, R. R.; Qin, A. J.; Tang, B. Z.; Su, B. Enhancing the visualization of latent fingerprints by aggregation induced emission of siloles. *Analyst* **2014**, *139*, 2332−2335.

[44] Hong, Y. N.; Lam, J. W. Y.; Tang, B. Z. Aggregation-induced emission. *Chem. Soc. Rev.* **2011**, *40*, 5361–5388.

[45] Jin, X. D.; Dong, L. B.; Di, X. Y.; Huang, H.; Liu, J. N.; Sun, X. L.; Zhang, X. Q.; Zhu, H. J. NIR luminescence for the detection of latent fingerprints based on ESIPT and AIE processes. *RSC Adv.* **2015**, *5*, 87306–87310.

[46] Jin, X. D.; Xin, R.; Wang, S. F.; Yin, W. Z.; Xu, T. X.; Jiang, Y.; Ji, X. R.; Chen, L. Y.; Liu, J. N. A tetraphenylethene-based dye for latent fingerprint analysis. *Sensor. Actuat. B: Chem.* **2017**, *244*, 777–784.

[47] Malik, A. H.; Kalita, A.; Iyer, P. K. Development of well-preserved, substrate-versatile latent fingerprints by aggregation-induced enhanced emission-active conjugated polyelectrolyte. *ACS Appl. Mater. Interfaces* **2017**, *9*, 37501−37508.

[48] Zhu, C. L.; Liu, L. B.; Yang, Q.; Lv, F. T.; Wang, S. Water-soluble conjugated polymers for imaging, diagnosis, and therapy. *Chem. Rev.* **2012**, *112*, 4687−4735.

[49] Bentolila, A.; Totre, J.; Zozulia, I.; Levin-Elad, M.; Domb, A. J. Fluorescent cyanoacrylate monomers and polymers for fingermark development. *Macromolecules* **2013**, *46*, 4822−4828.

[50] Lee, J.; Pyo, M.; Lee, S.-H.; Kim, J.; Ra, M.; Kim, W.-Y.; Park, B. J.; Lee, C. W.; Kim, J.-M. Hydrochromic conjugated polymers for human sweat pore mapping. *Nat. Commun.* **2014**, *5*, 3736.

[51] Locard, E. Les Pores et L'identification des criminels. *Biologica: Revue Scientifique de Medicine* **1912**, *2*, 357–365.

[52] Kwak, G.; Lee, W.-E.; Kim, W.-H.; Lee, H. Fluorescence imaging of latent fingerprints on conjugated polymer films with large fractional free volume. *Chem. Commun.* **2009**, 2112–2114.

[53] Chen, H. B.; Chang, K. W.; Men, X. J.; Sun, K.; Fang, X. F.; Ma, C.; Zhao, Y. X.; Yin, S. Y.; Qin, W. P.; Wu, C. F. Covalent patterning and rapid visualization of latent fingerprints with photo-cross-linkable semiconductor polymer dots. *ACS Appl. Mater. Interfaces* **2015**, *7*, 14477−14484.

[54] Chen, Y.-H.; Kuo, S.-Y.; Tsai, W.-K.; Ke, C.-S.; Liao, C.-H.; Chen, C.-P.; Wang, Y.-T.; Chen, H.-W.; Chan, Y.-H. Dual colorimetric and fluorescent imaging of latent fingerprints on both porous and nonporous surfaces with near-infrared fluorescent semiconducting polymer dots. *Anal. Chem.* **2016**, *88*, 11616–11623.

[55] Park, D.-H.; Park, B. J.; Kim, J.-M. Hydrochromic approaches to mapping human sweat pores. *Acc. Chem. Res.* **2016**, *49*, 1211−1222.

[56] Yoon, J.-H.; Jin, Y.-J.; Sakaguchi, T.; Kwak, G. Visualization of sweat fingerprints on various surfaces using a conjugated polyelectrolyte. *ACS Appl. Mater. Interfaces* **2016**, *8*, 24025–24029.

[57] Lee, J.; Lee, C. W.; Kim, J.-M. A magnetically responsive polydiacetylene precursor for latent fingerprint analysis. *ACS Appl. Mater. Interfaces* **2016**, *8*, 6245−6251.

[58] Kim, B. S.; Jin, Y.-J.; Uddin, M. A.; Sakaguchi, T.; Woo, H. Y.; Kwak, G. Surfactant chemistry for fluorescence imaging of latent fingerprints using conjugated polyelectrolyte nanoparticles. *Chem. Commun.* **2015**, *51*, 13634–13637.

[59] Pyo, M.; Lee, J.; Baek, W.; Lee, C. W.; Park, B. J. Kim, J.-M. Sweat pore mapping using a fluorescein-polymer composite film for fingerprint analysis. *Chem. Commun.* **2015**, *51*, 3177–3180.

[60] Yang, S. Y.; Wang, C.-F.; Chen, S. A release-induced response for the rapid recognition of latent fingerprints and formation of inkjet-printed patterns. *Angew. Chem., Int. Ed.* **2011**, *50*, 3706–3709.

[61] Zhang, S. J.; Liu, R. H.; Cui, Q. L.; Yang, Y.; Cao, Q.; Xu, W. Q.; Li, L. D. Ultrabright fluorescent silica nanoparticles embedded with conjugated oligomers and their application in latent fingerprint detection. *ACS Appl. Mater. Interfaces* **2017**, *9*, 44134−44145.

[62] Kim, Y.-J.; Jung, H.-S.; Lim, J.; Ryu, S.-J.; Lee, J.-K. Rapid imaging of latent fingerprints using biocompatible fluorescent silica nanoparticles. *Langmuir* **2016**, *32*, 8077−8083.

[63] Cho, E. C.; Glaus, C.; Chen, J. Y.; Welch, M. J.; Xia, Y. N. Inorganic nanoparticle-based contrast agents for molecular imaging. *Trends Mol. Med.* **2010**, *16*, 561−573.

[64] Leggett, R.; Lee-Smith, E. E.; Jickells, S. M.; Russell, D. A. "Intelligent" fingerprinting: Simultaneous identification of drug metabolites and individuals by using antibody-functionalized nanoparticles. *Angew. Chem., Int. Ed.* **2007**, *46*, 4100–4103.

[65] Menzel, E. R.; Takatsu, M.; Murdock, R. H.; Bouldin, K.; Cheng, K. H. Photoluminescent CdS/dendrimer nanocomposites for fingerprint detection. *J. Forensic Sci.* **2000**, *45*, 770–773.

[66] Xu, C. Y.; Zhao, R. H.; He, W. W.; Wu, L.; Wu, P.; Hou, X. D. Fast imaging of eccrine latent fingerprints with nontoxic Mn-doped ZnS QDs. *Anal. Chem.* **2014**, *86*, 3279−3283.

[67] Gao, F.; Lv, C. F.; Han, J. X.; Li, X. Y.; Wang, Q.; Zhang, J.; Chen, C.; Li, Q.; Sun, X. F.; Zheng, J. C. et al. CdTe–montmorillonite nanocomposites: Control synthesis, UV radiation-dependent photoluminescence, and enhanced latent fingerprint detection. *J. Phys. Chem. C* **2011**, *115*, 21574–21583.

[68] Cai, K. Y.; Yang, R. Q.; Wang, Y. J.; Yu, X. J.; Liu, J. J. Super fast detection of latent fingerprints with water soluble CdTe quantum dots. *Forensic Sci. Int.* **2013**, *226*, 240−243.

[69] Moret, S.; Bécue, A.; Champod, C. Cadmium-free quantum dots in aqueous solution: Potential for fingermark detection, synthesis and an application to the detection of fingermarks in blood on non-porous surfaces. *Forensic Sci. Int.* **2013**, *224*, 101−110.

[70] Algarra, M.; Jiménez-Jiménez, J.; Miranda, M. S.; Campos, B. B.; Moreno-Tost, R.; Rodriguez-Castellón, E.; Esteves da Silva, J. C. G. Solid luminescent CdSe-thiolated porous phosphate heterostructures. Application in fingermark detection in different surfaces. *Surf. Interface Anal.* **2013**, *45*, 612–618.

[71] Wu, P.; Hou, X. D.; Xu, J.-J.; Chen, H.-Y. Ratiometric fluorescence, electrochemiluminescence, and photoelectrochemical chemo/biosensing based on semiconductor quantum dots. *Nanoscale* **2016**, *8*, 8427−8442.

[72] Li, Y. Q.; Xu, C. Y.; Shu, C.; Hou, X. D.; Wu, P. Simultaneous extraction of level 2 and level 3 characteristics from latent fingerprints imaged with quantum dots for improved fingerprint analysis. *Chin. Chem. Lett.* **2017**, *28*, 1961−1964.

[73] Qu, S. N.; Wang, X. Y.; Lu, Q. P.; Liu, X. Y.; Wang, L. J. A biocompatible fluorescent ink based on water-soluble luminescent carbon nanodots. *Angew. Chem., Int. Ed.* **2012**, *51*, 12215−12218.

[74] Chen, J.; Wei, J.-S.; Zhang, P.; Niu, X.-Q.; Zhao, W.; Zhu, Z.-Y.; Ding, H.; Xiong, H.-M. Red-emissive carbon dots for fingerprints detection by spray method: Coffee ring effect and unquenched fluorescence in drying process. *ACS Appl. Mater. Interfaces* **2017**, *9*, 18429−18433.

[75] Dilag, J.; Kobus, H.; Yu, Y.; Gibson, C. T.; Ellis, A. V. Non-toxic luminescent carbon dot/poly (dimethylacrylamide) nanocomposite reagent for latent fingermark detection synthesized via surface initiated reversible addition fragmentation chain transfer polymerization. *Polym. Int.* **2015**, *64*, 884–891.

[76] Zhao, Y.-B.; Ma, Y.-J.; Song, D.; Liu, Y.; Luo, Y. P.; Lin, S.; Liu, C.-Y. New luminescent nanoparticles based on carbon dots/SiO_2 for the detection of latent fingermarks. *Anal. Methods* **2017**, *9*, 4770–4775.

[77] Wu, P.; Xu, C. Y.; Hou, X. D.; Xu, J.-J.; Chen, H.-Y. Dual-emitting quantum dot nanohybrid for imaging of latent fingerprints: Simultaneous identification of individuals and traffic light-type visualization of TNT. *Chem. Sci.* **2015**, *6*, 4445–4450.

[78] Dilag, J.; Kobus, H.; Ellis, A. V. Cadmium sulfide quantum dot/chitosan nanocomposites for latent fingermark detection. *Forensic Sci. Int.* **2009**, *187*, 97–102.

[79] Ranjan, S; Jayakumar, M. K. G.; Zhang, Y. Luminescent lanthanide nanomaterials: An emerging tool for theranostic applications. *Nanomedicine* **2015**, *10*, 1477–1491.

[80] Wang, M.; Li, M.; Yu, A. Y.; Wu, J.; Mao, C. B. Rare earth fluorescent nanomaterials for enhanced development of latent fingerprints. *ACS Appl. Mater. Interfaces* **2015**, *7*, 28110−28115.

[81] Chen, C. L.; Yu, Y.; Li, C. G.; Liu, D.; Huang, H.; Liang, C.; Lou, Y.; Han, Y.; Shi, Z.; Feng, S. H. Facile synthesis of highly water-soluble lanthanide-doped t-$LaVO_4$ NPs for antifake ink and latent fingermark detection. *Small* **2017**, *13*, 1702305.

[82] Tedstone, A. A.; Lewis, D. J.; O'Brien, P. Synthesis, properties, and applications of transition metal-doped layered transition metal dichalcogenides. *Chem. Mater.* **2016**, *28*, 1965−1974.

[83] Wu, P.; Pan, J.-B.; Li, X.-L.; Hou, X. D.; Xu, J.-J.; Chen, H.-Y. Long-lived charge carriers in Mn-doped CdS quantum dots for photoelectrochemical cytosensing. *Chem.—Eur. J.* **2015**, *21*, 5129–5135.

[84] Wang, J.; Ma, Q. Q.; Liu, H. Y.; Wang, Y. Q.; Shen, H. J.; Hu, X. X.; Ma, C.; Yuan, Q.; Tan, W. H. Time-gated imaging of latent fingerprints and specific visualization of protein secretions via molecular recognition. *Anal. Chem.* **2017**, *89*, 12764−12770.

[85] Mathew, A.; Pradeep, T. Noble metal clusters: Applications in energy, environment, and biology. *Part. Part. Syst. Charact.* **2014**, *31*, 1017–1053.

[86] Teng, Y.; Jia, X. F.; Zhang, S.; Zhu, J. B.; Wang, E. K. A nanocluster beacon based on the template transformation of DNA-templated silver nanoclusters. *Chem. Commun.* **2016**, *52*, 1721–1724.

[87] Ran, X.; Wang, Z. Z.; Zhang, Z. J.; Pu, F.; Ren, J. S.; Qu, X. G. Nucleic-acid-programmed Ag-nanoclusters as a generic platform for visualization of latent fingerprints and exogenous substances. *Chem. Commun.* **2016**, *52*, 557–560.

[88] Becue, A.; Scoundrianos, A.; Champod, C.; Margot, P. Fingermark detection based on the *in situ* growth of luminescent nanoparticles—Towards a new generation of multimetal deposition. *Forensic Sci. Int.* **2008**, *179*, 39–43.

[89] Jaber, N.; Lesniewski, A.; Gabizon, H.; Shenawi, S.; Mandler, D.; Almog, J. Visualization of latent fingermarks by nanotechnology: Reversed development on paper—A remedy to the variation in sweat composition. *Angew. Chem., Int. Ed.* **2012**, *51*, 12224–12227.

[90] He, Y. Y.; Xu, L. R.; Zhu, Y.; Wei, Q. H.; Zhang, M. Q.; Su, B. Immunological multimetal deposition for rapid visualization of sweat fingerprints. *Angew. Chem., Int. Ed.* **2014**, *53*, 12609–12612.

[91] van Dam, A.; Aalders, M. C. G.; van Leeuwen, T. G.; Lambrechts, S. A. G. The compatibility of fingerprint visualization techniques with immunolabeling. *J. Forensic Sci.* **2013**, *58*, 999–1002.

[92] van Dam, A.; van Nes, K. A.; Aalders, M. C. G.; van Leeuwen, T. G.; Lambrechts, S. A. G. Immunolabeling of fingermarks left on forensic relevant surfaces, including thermal paper. *Anal. Methods* **2014**, *6*, 1051–1058.

[93] Spindler, X.; Hofstetter, O.; McDonagh, A. M.; Roux, C.; Lennard, C. Enhancement of latent fingermarks on non-porous surfaces using anti-L-amino acid antibodies conjugated to gold nanoparticles. *Chem. Commun.* **2011**, *47*, 5602–5604.

[94] Hazarika, P.; Jickells, S. M.; Wolff, K.; Russell, D. A. Imaging of latent fingerprints through the detection of drugs and metabolites. *Angew. Chem., Int. Ed.* **2008**, *47*, 10167–10170.

[95] Hazarika, P.; Jickells, S. M.; Wolff, K.; Russell, D. A. Multiplexed detection of metabolites of narcotic drugs from a single latent fingermark. *Anal. Chem.* **2010**, *82*, 9150–9154.

[96] Hazatika, P.; Jickells, S. M.; Russell, D. A. Rapid detection of drug metabolites in latent fingermarks. *Analyst* **2009**, *134*, 93–96.

[97] Boddis, A. M.; Russell, D. A. Simultaneous development and detection of drug metabolites in latent fingermarks using antibody–magnetic particle conjugates. *Anal. Methods* **2011**, *3*, 519–523.

[98] Boddis, A. M.; Russell, D. A. Development of aged fingermarks using antibody-magnetic particle conjugates. *Anal. Methods* **2012**, *4*, 637–641.

[99] Akiba, N.; Kuroki, K.; Kurosawa, K.; Tsuchiya, K. Visualization of aged fingerprints with an ultraviolet laser. *J. Forensic Sci.* **2018**, *63*, 556–562.

[100] Matsuzawa, T.; Aoki, Y.; Takeuchi, N.; Murayama, Y. A new long phosphorescent phosphor with high brightness, $SrAl_2O_4:Eu^{2+},Dy^{3+}$. *J. Electrochem. Soc.* **1996**, *143*, 2670–2673.

[101] Li, Y.; Gecevicius, M.; Qiu, J. R. Long persistent phosphors—From fundamentals to applications. *Chem. Soc. Rev.* **2016**, *45*, 2090−2136.

[102] Li, Z. J.; Zhang, Y. W.; Wu, X.; Huang, L.; Li, D. S.; Fan, W.; Han, G. Direct aqueous-phase synthesis of sub-10 nm "luminous pearls" with enhanced *in vivo* renewable near-infrared persistent luminescence. *J. Am. Chem. Soc.* **2015**, *137*, 5304−5307.

[103] Wang, J.; Ma, Q. Q.; Hu, X.-X.; Liu, H. Y.; Zheng, W.; Chen, X. Y.; Yuan, Q.; Tan, W. H. Autofluorescence-free targeted tumor imaging based on luminous nanoparticles with composition-dependent size and persistent luminescence. *ACS Nano* **2017**, *11*, 8010−8017.

[104] Wang, J.; Ma, Q. Q.; Zheng, W.; Liu, H. Y.; Yin, C. Q.; Wang, F. B.; Chen, X. Y.; Yuan, Q.; Tan, W. H. One-dimensional luminous nanorods featuring tunable persistent luminescence for autofluorescence-free biosensing. *ACS Nano* **2017**, *11*, 8185−8191.

[105] Wang, J.; Ma, Q. Q.; Wang, Y. Q.; Shen, H. J.; Yuan, Q. Recent progress in biomedical applications of persistent luminescence nanoparticles. *Nanoscale* **2017**, *9*, 6204–6218.

[106] Liu, H. Y.; Hu, X. X.; Wang, J.; Liu, M.; Wei, W.; Yuan, Q. Direct low-temperature synthesis of ultralong persistent luminescence nanobelts based on a biphasic solution-chemical reaction. *Chin. Chem. Lett.*, in press, https://doi.org/10.1016/j.cclet.2018.02.005.

[107] Baffou, G.; Quidant, R. Nanoplasmonics for chemistry. *Chem. Soc. Rev.* **2014**, *43*, 3898−3907.

[108] Anker, J. N.; Hall, W. P.; Lyandres, O.; Shah, N. C.; Zhao, J.; van Duyne, R. P. Biosensing with plasmonic nanosensors. *Nat. Mater.* **2008**, *7*, 442−453.

[109] Li, K.; Qin, W. W.; Li, F.; Zhao, X. C.; Jiang, B. W.; Wang, K.; Deng, S. H.; Fan, C. H.; Li, D. Nanoplasmonic imaging of latent fingerprints and identification of cocaine. *Angew. Chem., Int. Ed.* **2013**, *52*, 11542–11545.

[110] Elghanian, R.; Storhoff, J. J.; Mucic, R. C.; Letsinger, R. L.; Mirkin, C. A. Selective colorimetric detection of polynucleotides based on the distance-dependent optical properties of gold nanoparticles. *Science* **1997**, *277*, 1078–1081.

[111] Song, K.; Huang, P.; Yi, C. L.; Ning, B.; Hu, S.; Nie, L. M.; Chen, X. Y.; Nie, Z. H. Photoacoustic and colorimetric visualization of latent fingerprints. *ACS Nano* **2015**, *9*, 12344–12348.

[112] Peng, T. H.; Qin, W. W.; Wang, K.; Shi, J. Y.; Fan, C. H.; Li, D. Nanoplasmonic imaging of latent fingerprints with explosive RDX residues. *Anal. Chem.* **2015**, *87*, 9403−9407.

[113] Li, W. W.; Chen, X. Y. Gold nanoparticles for photoacoustic imaging. *Nanomedicine* **2015**, *10*, 299–320.

[114] Zhao, L.; Wang, W.; Hu, W. H. Simultaneous transfer and imaging of latent fingerprints enabled by interfacial separation of polydopamine thin film. *Anal. Chem.* **2016**, *88*, 10357−10361.

[115] Zhao, L.; Huang, X. Q.; Hu, W. H. Interfacial separation-enabled all-dry approach for simultaneous visualization, transfer, and enhanced Raman analysis of latent fingerprints. *ACS Appl. Mater. Interfaces* **2017**, *9*, 37350−37356.

[116] Zhang, Y. Y.; Zhou, W.; Xue, Y.; Yang, J.; Liu, D. B. Multiplexed imaging of trace residues in a single latent fingerprint. *Anal. Chem.* **2016**, *88*, 12502−12507.

[117] Zhao, J. J.; Zhang, K.; Li, Y. X.; Ji, J.; Liu, B. H. High-resolution and universal visualization of latent fingerprints based on aptamer-functionalized core−shell nanoparticles with embedded SERS reporters. *ACS Appl. Mater. Interfaces* **2016**, *8*, 14389−14395.

[118] Song, W.; Mao, Z.; Liu, X. J.; Lu, Y.; Li, Z. S.; Zhao, B.; Lu, L. H. Detection of protein deposition within latent fingerprints by surface-enhanced Raman spectroscopy imaging. *Nanoscale* **2012**, *4*, 2333–2338.

[119] Cui, J. B.; Xu, S. Y.; Guo, C.; Jiang, R.; James, T. D.; Wang, L. Y. Highly efficient photothermal semiconductor nanocomposites for photothermal imaging of latent fingerprints. *Anal. Chem.* **2015**, *87*, 11592–11598.

[120] Hu, L. Z.; Xu, G. B. Applications and trends in electrochemiluminescence. *Chem. Soc. Rev.* **2010**, *39*, 3275–3304.

[121] Xu, L. R.; Li, Y.; Wu, S. Z.; Liu, X. H.; Su, B. Imaging latent fingerprints by electrochemiluminescence. *Angew. Chem., Int. Ed.* **2012**, *51*, 8068–8072.

[122] Xu, L. R.; Li, Y.; He, Y. Y.; Su, B. Non-destructive enhancement of latent fingerprints on stainless steel surfaces by electrochemiluminescence. *Analyst* **2013**, *138*, 2357–2362.

[123] Xu, L. R.; Zhou, Z. Y.; Zhang, C. Z.; He, Y. Y.; Su, B. Electrochemiluminescence imaging of latent fingermarks through the immunodetection of secretions in human perspiration. *Chem. Commun.* **2014**, *50*, 9097–9100.